Electronic Supplementary Material (ESI) for Journal of Materials Chemistry A.

Supplementary Information

Unlocking the potential of commercial carbon nanofibers as free-standing positive electrodes for flexible aluminum-ion batteries

Yuxiang Hu,[a] Shaikat Debnath,[b] Han Hu,[a] Bin Luo, *[a,d] Xiaobo Zhu,[a] Songcan Wang,[a] Marlies Hankel,[b] Debra J. Searles,[b, c] Lianzhou Wang *[a]

[a] Nanomaterials Centre, School of Chemical Engineering and Australian Institute for Bioengineering and Nanotechnology, The University of Queensland, St Lucia, QLD 4072, Australia. E-mail: b.luo1@uq.edu.au; l.wang@uq.edu.au

[b] Centre for Theoretical and Computational Molecular Science, Australian Institute for Bioengineering and Nanotechnology, The University of Queensland, Brisbane, QLD, 4072, Australia.

[c] School of Chemistry and Molecular Biosciences, The University of Queensland, Brisbane, QLD, 4072, Australia.

[d] State Key Laboratory Base of Eco-chemical Engineering, College of Chemical Engineering, Qingdao University of Science and Technology, Qingdao, 266042 China.

Experimental Section

GRCSs Preparation: The commercial CNFs produced by floating catalyst vapor-grown method was obtained from Merck (PR-25-XT-HHT, Conical carbon nanofibers). In a typical experiment, 500 mg raw CNFs was refluxed in a mixture of sulfuric acid and concentrated nitric acid (100ml, 3:1, *v/v*) at 70°C for 2h. The treated CNTs were filtered and washed three times with distilled water. The washed sample were then dried in a vacuum oven at 80°C overnight. The acid-treated CNFs were further annealed under H_2/N_2 (1:9, *v/v*) at 300°C for 1h. The obtained graphitic nanoribbon interconnected nanocup-stacks (GRCSs) was then used as electrode materials for AIBs assembling and measurements. For the preparation of free-standing GRCSs electrode, the acid-treated CNFs was dispersed in distilled water by sonication and then deposited on a cellulose membrane (Millipore VMWP, 0.05 μm pore size) by vacuum filtration and dried in a vacuum oven overnight. Finally, the free-standing film was obtained by dissolving the filtration membrane in acetone for 1 h.

AIBs Assembly: The free-standing GRCSs film directly utilized as the positive electrode in the AIBs. The natural graphite/GRCSs/CNFs was mixed with Carboxymethyl cellulose (CMC) (weight ratio of 9:1) in DI water and coated on molybdenum current collector followed by overnight high-vacuum heating under 100 °C. The ionic liquid (IL) electrolyte was prepared via mixing 1-ethyl-3-methylimidazolium chloride ([EMIm]Cl, 98%, Sigma) and anhydrous aluminum chloride (99.99%, Sigma-Aldrich) (mole ratio of 1.3). A glass fibre was applied as the separator (Whatman). The negative electrode electrode is the aluminum foil (Sigma-Aldrich, 99.999%).

Materials Characterization & Electrochemical Measurements: The samples were characterized with X-ray diffraction (XRD) (Bruker, Cu Kα, λ = 0.15406 nm, D8-Advance X-ray diffractometer,). Raman spectra were obtained via a Renishaw Micro-Raman Spectroscopy

System with a laser wavelength of 514 nm. The transmission electron microscopy (TEM), scanning electron microscopy (SEM) (JEOL-7001), and the high-resolution TEM (HR-TEM) (FEI F20 FEG-STEM) were used to characterize the morphology of samples. After 12 hours degassing at 150 °C, the specific surface area measurements were carried out on a Tristar nitrogen sorption instrument (Micrometrics Instrument Corporation) and calculated based on Brunauer–Emmet–Teller (BET) analysis.

The electrochemical performance of the GRCSs, CNFs, and natural graphite was tested by battery tester (LAND-CT2001A). The capacities are calculated based on the weight of active materials. The cyclic voltammogram (CV) were detected via electrochemical station (CHI 600E Shanghai, China) under a scan rate of 0.5 mV s^{-1}.

Computational Details: Density functional theory (DFT) calculations were carried out employing the Vienna ab initio Simulation Package (VASP).[1] The exchange correlation potential is described with projected augmented-wave pseudopotentials,[2] and Perdew-Bruke-Ernzerhof (PBE)[3] generalized gradient approximation. The energy cut off was set to 500 eV and the convergence criterion for the self-consistent field calculation was 10^{-06} eV. The force convergence criterion was set to -0.01 eV/Å. All calculations were spin-polarized and a Gaussian smearing of 0.05 was applied. DFT-D3 approach was used for the correction of van der Waals interactions for potential energy and interatomic forces.[4]

To simulate the edge-rich GRCSs in a simply way, a graphene sheet, graphene ribbon, and carbon nanotube (CNT) were employed in the calculations as exhibited in Fig. S4. The simulation is aiming to investigate the effect of typical features in the GRCSs such as edges, shorter intercalation length (nanoribbon model), and the curvature of the nanocup (CNT model) on the intercalation of the chloroaluminate ion. We also compared the simulation

results of GRCSs with normal graphene (graphene sheet). Fig. S4 shows the geometrically optimized unit cells of graphene, graphene ribbon and carbon nanotube. A vacuum unit cell of a = b = 14.8 Å, c = 20 Å was used for graphene sheet, whereas it was a = 30 Å, b = 14.86 Å and c = 20 Å for graphene ribbon and a = b = 35 Å, c = 17.5 Å for CNT.

The Brillouin zone was sampled with a gamma centered k-points mesh of 3×3×1, 1×2×1 and 1×1×3 points for graphene, graphene ribbon and CNT, respectively. Bader charge analysis and charge density differences were conducted to understand the charge transfer process between the chloroaluminate ions and the material.

The interaction of the chloroaluminate ion with the materials is represented by the binding energy following the equation (Eq. 1):

$$E_{\text{binding}} = E_{X+\text{AlCl4}} - E_{\text{X}} - E_{\text{AlCl4}} \qquad \text{(Eq. 1)}$$

where, X = graphene sheet/graphene ribbon/CNT, $E_{X+\text{AlCl4}}$ and E_X are the total energies of graphene sheet/graphene ribbon/CNT with or without $AlCl_4$ ion. E_{AlCl4} is the total energy of one $AlCl_4$ molecule. Based on this definition, a positive binding energy means a stable configuration and a favorable interaction, whereas a negative binding energy represents an unstable structural configuration.

To investigate the required energy for $AlCl_4$ ion intercalation, a bilayer system was employed. The simulation will also give an indication of the change in volume expansion compared to the pristine graphite. The $AlCl_4$ ion is too large to intercalate easily between the layers of the pristine material. After intercalation, the bilayers would be moved further apart. The energy needed for this volume change is represented by a distortion energy, which is defined as (Eq. 2):

$$E_{\text{distortion}} = E_{X1} - E_{X2} \qquad \text{(Eq. 2)}$$

Here, E_{X1} is the total energy of the bilayer system of graphene/graphene ribbon in natural

condition. E_{X2} is the total energy of the expanded bilayer system after $AlCl_4$ ion intercalation. The binding energy of the bilayer system after $AlCl_4$ ion intercalation can be described as the equation (Eq. 3):

$$E_{binding} = E_{X+AlCl4} - E_X - E_{AlCl4} - E_{distortion} \quad \text{(Eq. 3)}$$

Based on this definition, the binding energy for the first $AlCl_4$ ion intercalation into the bilayer system should be negative because as it includes the distortion energy to push the layers apart signifying that this process is not favourable. The distortion energy is an indication of the difficulty of $AlCl_4$ ion intercalation. A lower distortion energy means an easier intercalation between the layers.

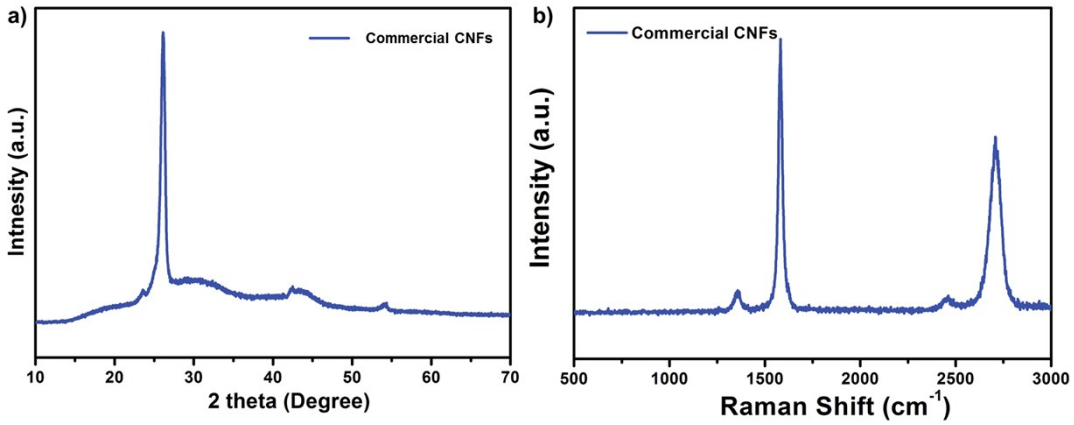

Fig. S1. a) XRD pattern of the commercial CNFs. b) Raman spectra of the commercial CNFs.

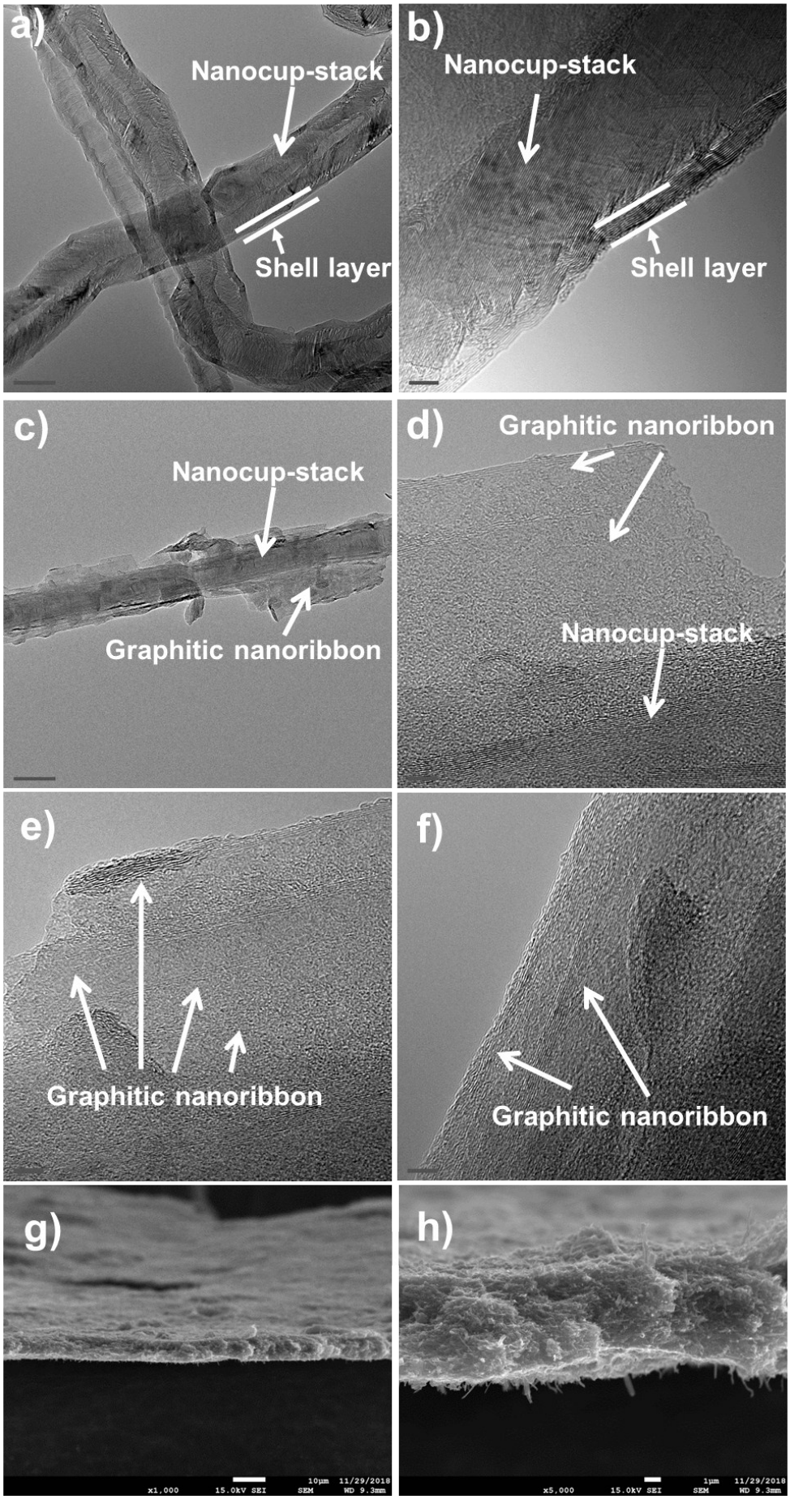
a)
Nanocup-stack
Shell layer
b)
Nanocup-stack
Shell layer
c)
Nanocup-stack
Graphitic nanoribbon
d)
Graphitic nanoribbon
Nanocup-stack
e)
Graphitic nanoribbon
f)
Graphitic nanoribbon
g)
10μm 11/29/2018
x1,000 15.0kV SEI SEM WD 9.3mm
h)
1μm 11/29/2018
x5,000 15.0kV SEI SEM WD 9.3mm

Fig. S2. a, b) TEM images of the commercial CNFs with the explanation of the nanocup-stack and carbon nanotube shell layer of the structure. Due to the few-layer carbon nanotube, the $AlCl_4$ ion was mostly hindered to de/intercalate into the well-fabricated nanocup-stacks. c-f) TEM images of the GRCSs after facile acid-treatment. It is clear to observe that the few layer carbon nanotubes are cleaved into nanoribbons, which are consisted by layered graphitic carbon and tactfully served as the high conductive substrate for the interior carbon nanocup-stacks. These graphitic nanoribbons will also contribute to the capacity in AIB indicated by previous literatures.[5, 6] Scale bar in the Figures a-f are 50nm, 5nm, 100 nm, 5 nm, 5 nm, and 5 nm, respectively. g, h) SEM images of the binder-free and free-standing GRCSs film. The presented film is around 5 μm with the well-retained GRCSs morphology.

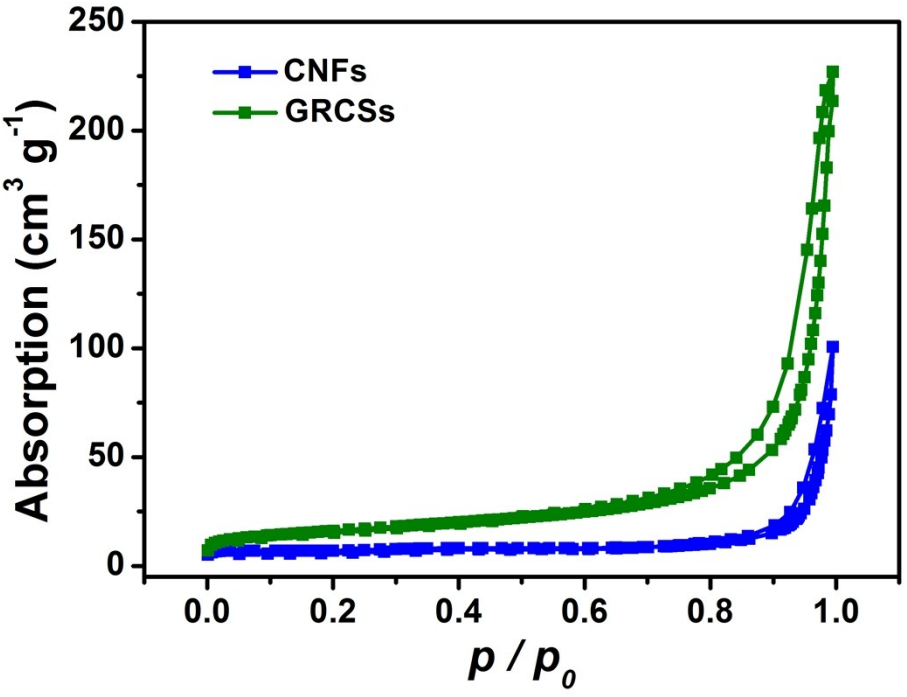

Fig. S3. N_2 adsorption–desorption isotherms of the CNFs (bule) and GRCSs (green). The BET specific surface area is 23.21 m^2 g^{-1} for CNFs and 55.26 m^2 g^{-1} for GRCSs. Compared with the surface area of the commercial CNFs, GRCSs exhibits larger reaction area, which can be favorable to the electrolyte penetration and ion/electron diffusion.

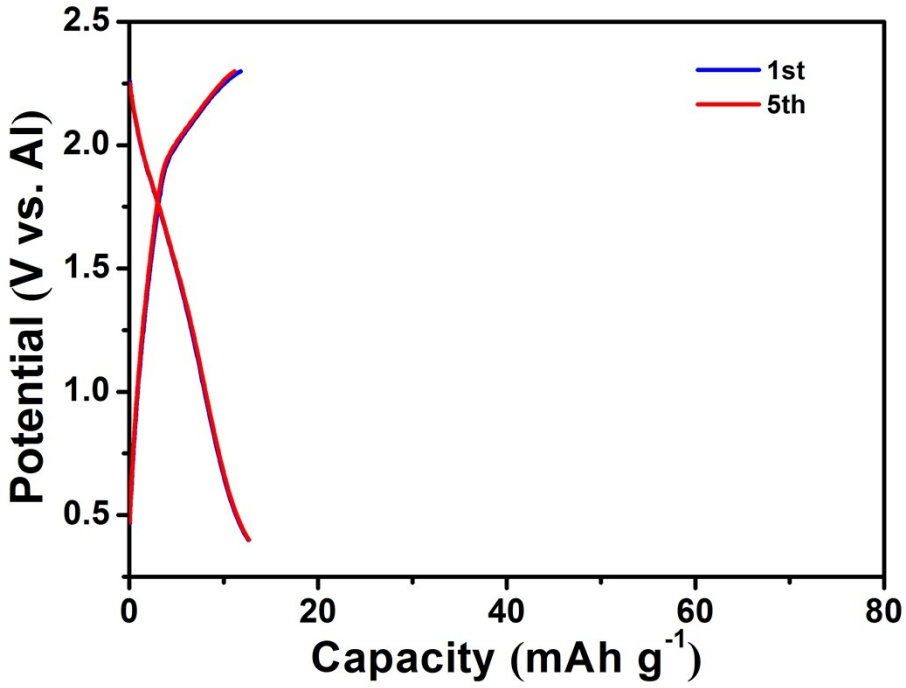

Fig. S4. Charge-discharge curves of the commerical CNFs at 1st and 5th cycle with less than 15 mAh g^{-1} capacity under the current density of 1 A g^{-1}.

Table S1 The comparison of energy density of various positive electrodes

Various Positive electrodes	Energy density (Wh kg^{-1}) under various current densities						
	0.5 A g^{-1}	1 A g^{-1}	2 A g^{-1}	5 A g^{-1}	10 A g^{-1}	20 A g^{-1}	50 A g^{-1}
GRCSs		214.2	210.8	187	177.31	166.6	160.14
CVD-Graphene[7]	108.5	105	103.25	101.5	--	--	--
Graphene Foam[8]		184.3	185	182	172	160	150.1

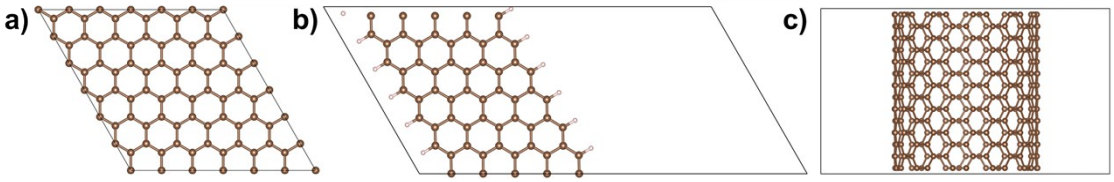

Fig. S5. Geometrically optimized structure of a) graphene sheet, b) edge-rich graphene ribbon, and c) CNT. The brown balls represent carbon and the light pink balls hydrogen.

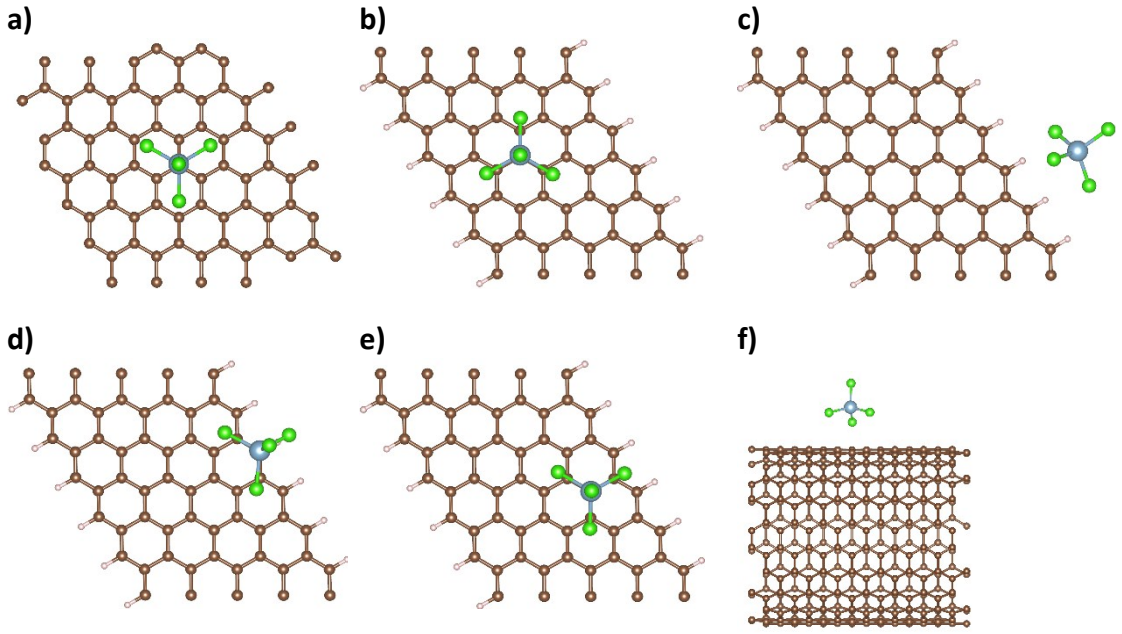

Fig. S6. DFT-based comparison between normal graphene, edge-rich graphene, and curved graphene (CNT). We have calculated the binding energies after placing $AlCl_4$ ion in different positions of single layer graphene, edge-rich graphene, and CNT. a) The $AlCl_4$ ion loading of graphene. Whereas b), c), d) and e) represents the loading of $AlCl_4$ ion in different positions of edge-rich graphene. f) represents the loading of $AlCl_4$ ion in curved graphene, where the carbon nanotube (CNT) is selected as the representive sturcture to simplify the simulation. The brown balls represent carbon, the light pink ones hydrogen, green balls are chlorines and the sky-blue ball aluminium.

To investigate the effect of the different structures on the intercalation of the $AlCl_4$ ion the ion was initially placed on a monolayer of graphene. Regarding graphene, the $AlCl_4$ ion adsorbs with an energy of 2.21 eV, Fig. S6a), which is consistent with the previous publications.[1, 2] The preferred position is shown in Fig. S6a) on graphene. Regarding the graphene ribbon model, the $AlCl_4$ ion was placed in the middle of the ribbon and then moved closer and beyond the edge as exhibited in Fig. S6 b-e).

DFT calculations have been carried out to compare the binding energy after placing chloroaluminate ions in different positions of graphene, edge-rich graphene and

curved graphene. The binding energies of b), c), d), and e) are 2.39 eV, 2.45 eV, 2.42eV and 2.38 eV, respectively. It is obvious that the binding energy for all the loading positions of the chloroaluminate ions onto edge-rich graphene are higher than that of graphene. Furthermore, the binding energy between the curved graphene (CNT) and the chloroaluminate ion is calculated as 2.54 eV, which is also higher than that of graphene as well. Hence it is clear that the two features of edge-rich and graphitic curvature, both contribute to the stronger binding between the $AlCl_4$ ion and GRCSs in comparison with that of normal graphene.

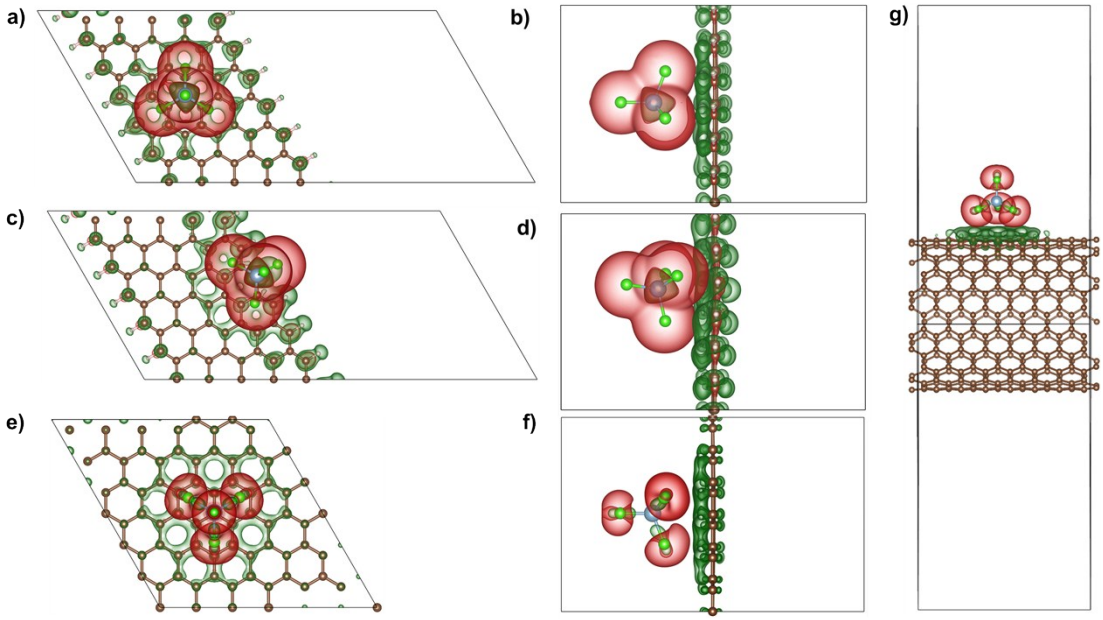

Fig. S7. Charge density difference calculations are conducted to observe the charge transfer between GRCSs layer and $AlCl_4$ ion. a) and b) represent the charge density difference of single layer graphene ribbon with $AlCl_4$ ion in middle a) top view and b) side view. c) and d) represent the charge density difference of single layer of GRCSs with $AlCl_4$ ion loaded at the edge c) top view and d) side view. Charge density difference calculations of chloroaluminate ions on graphene single layer, e) top view and f) side view. g) Charge density difference result of $AlCl_4$ ion on CNT. The red represents that electrons have been gained and green represents that electrons have been lost. An isosurface level of 0.0007 $eÅ^{-3}$ was used in all images. The brown balls represent carbon, the light pink ones hydrogen, green balls are chlorines and the sky-blue ball aluminium.

Fig. S7 shows the charge transfer between chloroaluminate ions and graphene/ edge-rich graphene/CNT single layer. It is clear that the chloroaluminate ions gained electrons in all cases, whereas the normal graphene, CNT, or edge-rich graphene donated electrons. Bader charge calculation were carried out in all cases show that the chloroaluminate ion has gained almost one electron from the graphene/edge-rich graphene sheet/CNT.

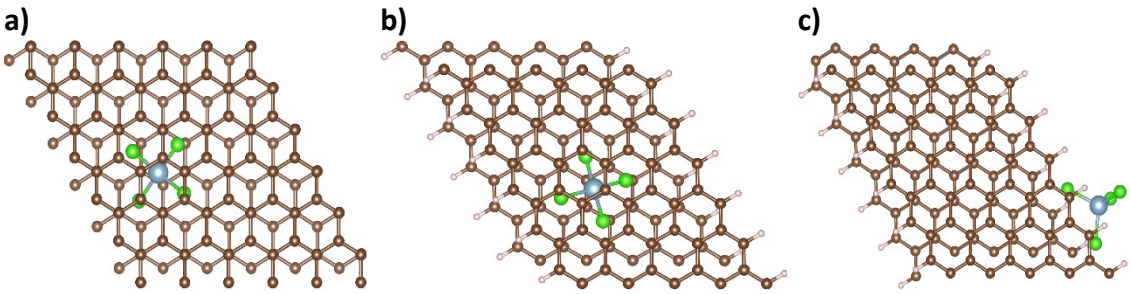

Fig. S8. Chloroaluminate ions are loaded in a) bilayer of graphene, b) in the middle of bilayer of edge-rich graphene and c) at the edge of bilayer of edge-rich graphene. Green, sky-blue, brown, and light pink balls represent chlorine, aluminum, carbon, and hydrogen, respectively.

To test the intercalation of the $AlCl_4$ ion into the different structures, the $AlCl_4$ ion was placed between the two layers of a bilayer system of graphene and the edge-rich graphene (Fig. S8). AB stacking configurations were used in all the cases. In the graphene and edge-rich graphene bilayer systems, the $AlCl_4$ ion re-orientates into a lying position. It is different from the single layer system, where it orients in a standing tetrahedral position also found in previous theoretical studies.[1-3] Based on DFT calculation, the binding energies of a), b) and c) are found as -3.14 eV, -1.66 eV and -1.17eV respectively. The negative energy indicates that the intercalation of the first $AlCl_4$ ion is not favorable. Compared with that of the normal graphene system, the intercalation is more favorable in the edge-rich graphene system with less negative energy (about 1.58 eV). Herein, it is evident that $AlCl_4$ ion prefers to intercalate between the edge-rich graphene bilayers. The most preferred position for $AlCl_4$ ion is to sit at the edge between two layers of finite edged graphene.

Meanwhile, the distortion energy, defined as the required energy to push the two layers apart, have also been calculated. In edge-rich graphene, the distortion energy is found as 2.16 eV, which is lower than that of graphene (3.14 eV). The result indicates that less energy is needed for the edge-rich bilayer graphene to accomdate $AlCl_4$ ion in comparison with that of normal graphene. Note that, the layers have to

be apart around 9 Å to accomodate the chloroaluminate ions in both cases.

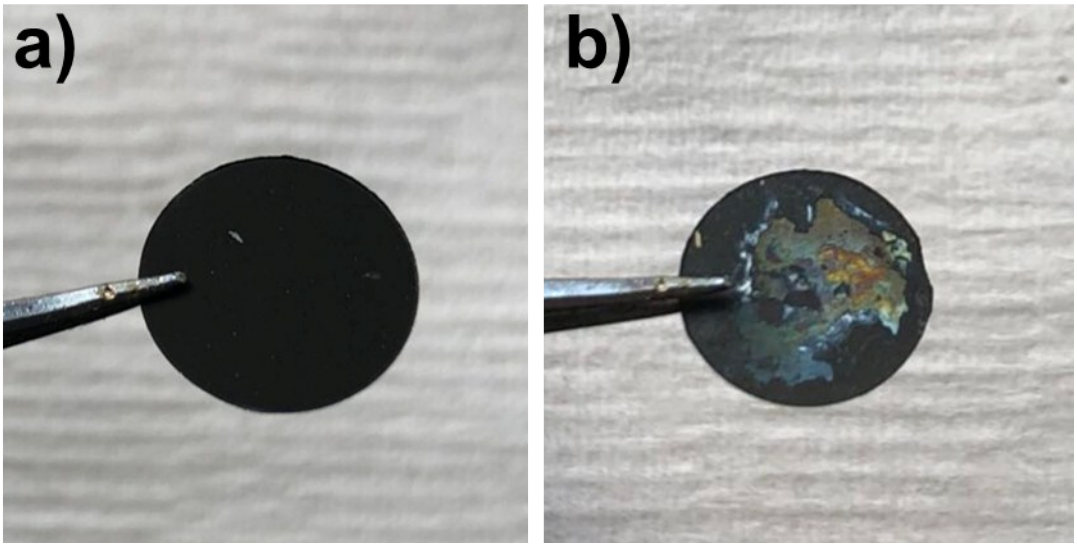

Fig. S9. Photograph of the electrode of commercial graphite loading on the Mo foil a) Pristine electrode and b) electrode after 2,000 cycles**.**

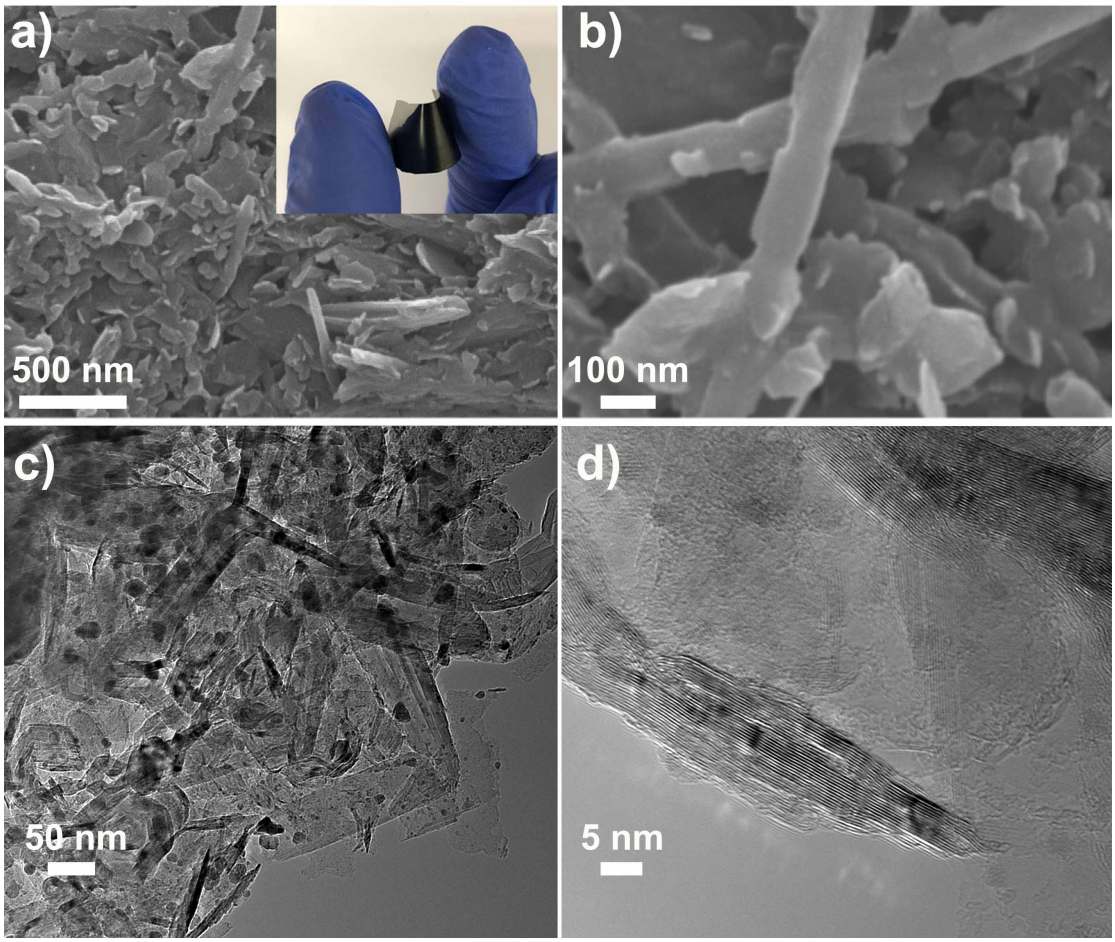

Fig. S10. a) and b) SEM images of the GRCSs after 2,000 cycles. The inset in a) exhibits the integrity of the cycled electrode after 2,000 cycles. c) TEM and d) HR-TEM image of the cycled GRCSs.

Reference

1. G. Kresse and J. Furthmüller, *Computational Materials Science*, 1996, **6**, 15-50.
2. P. E. Blöchl, *Physical Review B*, 1994, **50**, 17953-17979.
3. J. P. Perdew, K. Burke and M. Ernzerhof, *Physical Review Letters*, 1996, **77**, 3865-3868.
4. S. Grimme, J. Antony, S. Ehrlich and H. Krieg, *The Journal of Chemical Physics*, 2010, **132**, 154104.
5. S. K. Das, S. Mahapatra and H. Lahan, *J. Mater. Chem. A*, 2017, **5**, 6347-6367.
6. A. S. Childress, P. Parajuli, J. Zhu, R. Podila and A. M. Rao, *Nano Energy*, 2017, **39**, 69-76.
7. M. C. Lin, M. Gong, B. Lu, Y. Wu, D. Y. Wang, M. Guan, M. Angell, C. Chen, J. Yang, B. J. Hwang and H. Dai, *Nature*, 2015, **520**, 325-328.
8. H. Chen, F. Guo, Y. Liu, T. Huang, B. Zheng, N. Ananth, Z. Xu, W. Gao and C. Gao, *Adv. Mater.*, 2017, **29**, 1605958.